A New Sub-Doppler Fluorescence Imaging Method in Studying Laser Ablation of B Atoms at 248 nm

Jia-lin Chang,*,† Kuo-mei Chen,*,‡ Chun-hwa Sung,‡ Teng-hui Chung,‡ Kuo-huei Lee,‡ and Yit-Tsong Chen*,†,§

Institute of Atomic and Molecular Sciences, P.O. Box 23-166, Taipei 106, Taiwan, Republic of China, Department of Chemistry, National Sun Yat-sen University, Kaohsiung, Taiwan, Republic of China, and Department of Chemistry, National Taiwan University, Taipei 106, Taiwan, Republic of China

A new sub-Doppler fluorescence imaging method has been applied to study the laser ablation of B atoms at 248 nm with a power density of ~1.7×10^8 W/cm^2. Two-dimensional velocity distributions of the laser-ablated B($^2P^\circ_{1/2,3/2}$) atoms are measured. The angular distributions of the ablated B atoms are velocity-dependent; the higher the speed of the B atom is, the more centralized the distribution of the forward peaking will be, indicating that the ablation plume undergoes an unsteady adiabatic expansion. The speed distributions of the B atoms are well fitted to the shifted Maxwellian functions and are found to be bimodal, including a fast component with a temperature of 1.8×10^4 K topping out at 5.8 eV and a slow component of 3.1×10^3 K reaching a maximum at 2.8 eV. While a plasma reaction is responsible for the fast component, the slow one results from photochemical processes.

1. Introduction

Recently, we have developed a new "sub-Doppler fluorescence imaging" experimental technique to determine both velocity and angular distributions as well as vector correlations of state-selected photofragments.[1] This method combines Doppler-selection of velocities[2,3] and two-dimensional (2D) fluorescence imaging techniques,[4–10] thus being able to measure the 3D distributions of photofragments directly in the center-of-mass frame even with an uncollimated molecular beam. In addition, we have extended this method to study the mechanisms of laser ablation.

Laser ablation has been widely applied and investigated in the fields of chemistry, physics, biology, industry, and clinical applications.[11–14] For instance, a variety of thin films have been fabricated using laser ablation of solid materials, known as "pulsed laser deposition".[14] In fact, energetic atomic beams and jet-cooled cluster beams, which are difficult to be produced with other methods, can be generated by laser ablation to study the correlated spectroscopy and reaction dynamics. Furthermore, ablation with very high laser power usually results in the formation of high-energy plasmas, which can serve as a source of bright X-ray radiation.[11]

2. Experiment

Figure 1 depicts the experimental setup for determining the 2D velocity distributions of the laser-ablated B atoms. A boron rod was mounted on a motorized stage and placed inside a vacuum system (~10^{-6} Torr). The ablation beam with a wavelength of 248 nm from a KrF excimer laser, operated at a repetition rate of 1 Hz, was shaped by a circular iris ($\phi \approx 1$ cm) and then focused by a spherical lens ($f = 30$ cm) onto the
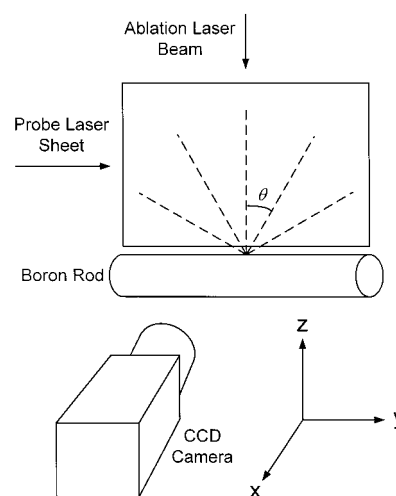
* Corresponding author.
† Institute of Atomic and Molecular Sciences.
‡ National Sun Yat-sen University.
§ National Taiwan University.

Figure 1. Schematic diagram of the experimental setup for the laser ablation of B atoms.

surface of the boron rod at a right angle. The diameter of the ablation spot is ~1 mm, produced from the 20-mJ ablation laser with pulse duration of ~15 ns. As a result, the power density at the focal spot was ~1.7×10^8 W/cm^2. The output of a dye laser, pumped by a XeCl excimer laser, with its frequency being doubled via a BBO crystal was used as a probe laser. This probe laser was expanded by an optical expander, comprising a concave and a convex lenses, and then focused by a cylindrical lens ($f \sim 50$ cm) to form a laser sheet (~$200\ \mu$m thick) with an effective probing area of ~2.8×4.0 cm^2. After a selected delay time to the ablation laser, the probe laser sheet, propagating parallel to the boron rod (Figure 1), was used to monitor the ablated ground-state B atoms through the laser-induced fluorescence (LIF) of the two spin–orbit components of B atom, i.e., B(3s ^{2}S) ← B(2p^{2}P$^\circ_{1/2,3/2}$) at 249.75 and 249.85 nm,[15] respectively. An intensified charge-coupled device (CCD)
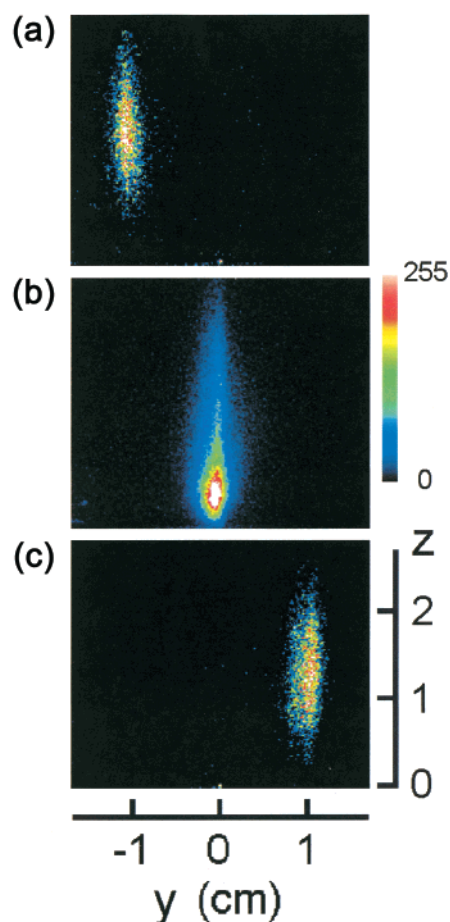
Figure 2. Images of the laser-ablated $B(^2P^\circ_{3/2})$ atoms probed at (a) $\nu_0 - 1.12$ cm^{-1}, (b) $\nu_0 = 40024.4$ cm^{-1}, and (c) $\nu_0 + 1.12$ cm^{-1}, with a delay time of 1.26 μs. The relative intensities of the fluorescence are represented by the false-color bar marked on the margin.

Figure 3. (a) Two-dimensional velocity distributions of the ablated $B(^2P^\circ_{3/2})$ atoms and (b) the corresponding contour plot.

camera focused on the plane of the laser sheet was utilized to detect the emitting fluorescence as a function of 2D spatial positions. After the rod surface was pretreated by a single laser pulse to remove impurities and oxides, the image was taken from averaging every five laser-shots at a Doppler-shifted frequency. A background image was also acquired as a reference when the probe laser was shut off. The boron rod was then moved ahead to provide fresh surface, and a similar measurement was performed at another probing frequency. The laser frequency was scanned through the whole Doppler profile to acquire all velocity information of the ablated B atoms within the yz plane. The recorded 2D images were the snapshots of the ablated B atoms controlled by the electronic shutter of a gated CCD with a pulse of 30 ns; the ablated B atoms were regarded as almost frozen within the lapse of pulse time.

3. Results and Discussion

Figure 2 shows three images of the $B(^2P^\circ_{3/2})$ atoms probed through the $B(^2S) \leftarrow B(^2P^\circ_{3/2})$ transitions at (a) $\nu_0 - 1.12$ cm^{-1}, (b) ν_0 (40024.4 cm^{-1}),[15] and (c) $\nu_0 + 1.12$ cm^{-1}, with a fixed delay time of 1.26 μs, which is slightly longer than that of the duration ($\sim$1.2 μs) of the luminous ablation plume. Preliminary and similar images of the $B(^2P^\circ_{1/2})$ atoms have been reported previously but without detailed analysis.[1] In this article, the extraction of 2D distributions of the ablated species from the full 3D space is analyzed as follows. First, the probe laser sheet slices the yz plane ($v_x = 0$) from the 3D space (Figure 1). Second, due to Doppler effect, the probe laser singles out the
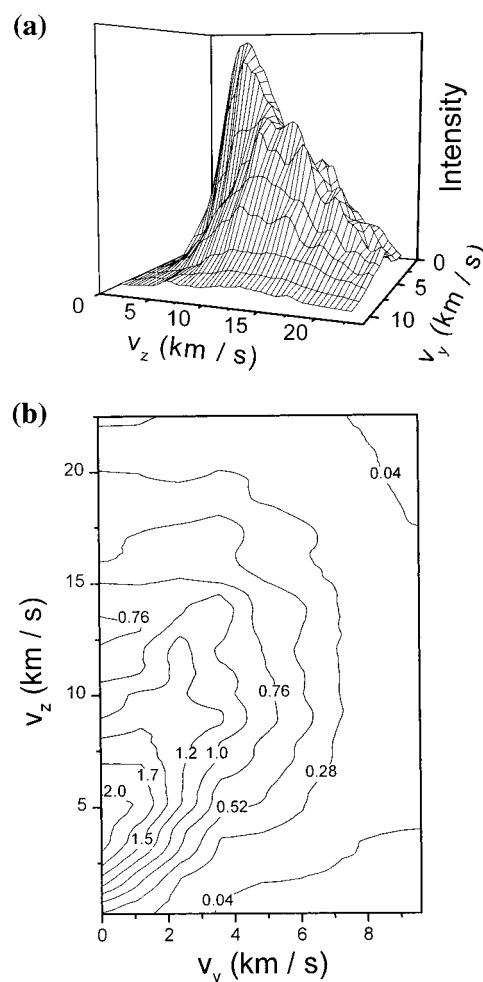
ablated species with $v_y = c(\nu - \nu_0)/\nu$, where c is the speed of light, ν is the laser frequency, and ν_0 is the Doppler-free atomic or molecular transition frequency. Accordingly, panels a−c of Figure 2 correspond to the ablated B atoms with $v_y = -8.4$, 0, and 8.4 km/s, respectively. Finally, v_z is determined from measuring $v_z = z/t$, where z is position of the recorded image and t is the time-of-flight of the ablated species. In general, the image patterns should be forward along the z-direction, with a finite width in the y-direction (Figure 2). Since the laser pulse durations ($\sim$15 ns) are very short relative to the delay time in this experiment, t is taken simply as the delay time between two pulsed lasers. The image width in the y-direction (Figure 2) is mainly caused by the bandwidth ($\sim$0.2 cm^{-1}) of the probe laser for velocity selectivity.

Figure 3a shows the 2D velocity distributions of the ablated $B(^2P^\circ_{3/2})$ atoms, and Figure 3b is the corresponding contour plot. In correlating the 2D velocity distributions (Figure 3) of the B atoms to the ablation mechanism, we have fitted the experimental data to conventional distribution functions in terms of scattering angle and speed. The angular distributions of the ablated B atoms, analyzed with the speed intervals of 1 km/s after transforming the Cartesian coordinates of Figure 3 into the corresponding polar coordinates, were fitted to the following equation:

$$P(\theta) = A[a \cos \theta + (1 - a) \cos^n \theta] \qquad (1)$$

where $P(\theta)$ is the angular distribution function, A is an adjustable
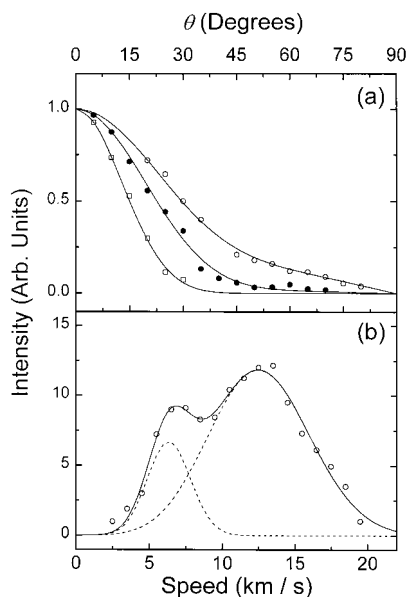
Letters

J. Phys. Chem. B, Vol. 105, No. 22, 2001 **5081**

Figure 4. (a) Angular distributions of the ablated B(^{2}P$^\circ_{3/2}$) atoms with average speeds of $\langle v \rangle = 2.5$ (open circles), 11.5 (filled circles), and 18.5 km/s (open squares), corresponding to the best-fit functions of $0.25 \cos \theta + 0.75 \cos^7 \theta$, $0.03 \cos \theta + 0.97 \cos^{11} \theta$, and $\cos^{20} \theta$ (solid lines), respectively. (b) Speed distributions of the ablated B(^{2}P$^\circ_{3/2}$) atoms (open circles), which match well with the shifted Maxwellian functions (solid line) containing two components (dashed lines).

constant, a is a coefficient ranging from 0 to 1, n is an integer, and θ is the ejection polar angle (Figure 1) of the B atoms relative to the surface normal. Theoretically, eq 1 can be used to describe bimodal angular distributions of laser-ablated species which are produced from both thermal ($\cos \theta$) and nonthermal processes ($\cos^n \theta$).[16] Figure 4a illustrates the angular distributions for the ablated B atoms with average speeds $\langle v \rangle = 2.5$, 11.5, and 18.5 km/s, which correspond to the distributions of $0.25 \cos \theta + 0.75 \cos^7 \theta$, $0.03 \cos \theta + 0.97 \cos^{11} \theta$, and $\cos^{20} \theta$, respectively. It can be seen from Figure 4a (or Figure 3b) that the angular distributions of the ablated B atoms are velocity-dependent. That is, the higher the speed of B atom, the more centralized is the distribution of the forward peaking, indicating that the ablation plume undergoes an unsteady adiabatic expansion.[14,16]

The speed distributions of the ablated B atoms were obtained by first taking the area covered by the best-fit angular distribution function in each speed interval and then multiplying this value by a factor of V_s/V_p ($\propto v$), where V_s is the volume of the hemispherical shell occupied by the ablated B atoms having average speed v and V_p is the volume of the shell sliced by the probe laser sheet. Consequently, the relative populations of B atoms pertinent to and within each speed interval were obtained. In our treatment, a cylindrical symmetry around the z-axis has been assumed. The assumption was justified by imaging the luminous ablation plumes from either the x- or the y-direction, where both images have shown to be the same within experimental uncertainties. More importantly, the speed distributions of the ablated B atoms consist very well with the shifted Maxwellian function, including two components

$$P(v) = c_1 v^2 \exp[-m(v - v_1)^2/2kT_1] +$$
$$c_2 v^2 \exp[-m(v - v_2)^2/2kT_2] \quad (2)$$

where $P(v)$ is the speed distribution function, c_1 and c_2 are adjustable constants, v_1 and v_2 are stream velocities, T_1 and T_2 are temperatures, k is the Boltzmann constant, and m is the mass

of the B atom. In other words, the speed distributions of the ablated B atoms are found to be bimodal comprising fast and slow components (Figure 4b). Predominantly, the fast component has been determined to be $(1.8 \pm 0.3) \times 10^4$ K, topping out at 5.8 eV, whereas the slow one is $(3.1 \pm 0.8) \times 10^3$ K, peaking at 2.8 eV.

The mechanisms of the laser ablation of B atoms at 248 nm can be delineated by the angular and speed distributions of the ablated B atoms.[11-14] The fast component, preferentially directing along the surface normal ($a = 0$ and $n = 12-25$) with an average kinetic energy of 5.8 eV, is generated via a plasma mechanism. The formation of plasma in this experiment is supported by the visible ablation plume, where the emission spectra (not shown) were analyzed to have a continuous and featureless band in the range of 200–700 nm. Within the pulse duration of the ablation laser, the electrons in the plasma are accelerated via an inverse Bremsstrahlung mechanism.[12] As soon as the laser field terminates, the plasma expands into the vacuum and the energetic neutral B atoms are produced from the recombination of B$^+$ ions with electrons. Part of the ground-state B atoms are relaxed from excited Rydberg states evidenced by their emission spectra, in which the transitions of B(3s ^{2}S) $\rightarrow$ B(2p^{2}P$^\circ_{1/2,3/2}$) were observed at 249.8 nm as a strong peak on the top of a continuous band, as mentioned above. Due to vigorous collisions of the ablated B atoms within the system, these species produced from plasma are usually of strong forward peaking.

The slow component spans more widely in space than the fast one does and is composed of a broad $\cos \theta$ and a narrow $\cos^n \theta$ angular distribution. The $\cos^n \theta$ term, however, dominates the angular distributions, meaning that the gas-dynamic effects also play an important role in the slow component, since intraplume collisions usually lead to the distribution of forward peaking.[16] The photochemical mechanism is responsible for the generation of the slow component, which is peaked at 2.8 eV, with angular distributions dominated by the $\cos^n \theta$ ($n = 6-11$). In other words, the ablated B atoms corresponding to the slow component are produced from the process of photodissociation of boron clusters or cluster ions via (multi)photon absorption. The formation of boron clusters and cluster ions was reported previously in the laser ablation of boron targets.[17,18] On the other hand, thermal evaporation is ruled out as the mechanism for generating the slow component because the $\cos^n \theta$ term, rather than the $\cos \theta$ term, dominates the angular distributions. It is the $\cos \theta$ term that is expected for a thermal process.[14,16] Furthermore, from fitting the Maxwell–Boltzmann (thermal) distribution function, an unusually high temperature of 5.9×10^4 K is obtained and would be inappropriate to account for a thermal process. The minor contribution from the $\cos \theta$ term, appearing in the wings of the angular distributions for the low-velocity species, can be attributed to the ablated B atoms undergoing few or no collisions.[14,16]

In contrast to the photodissociation experiment using an uncollimated molecular beam,[1] the bandwidth of the probe laser is in fact not necessary to be sub-Doppler for the experiment with pulsed laser ablation, where a focused laser spot has clearly defined the spatial origin for all of the ablated products. Generally, it is more efficient to record and average the image while scanning laser frequency through the whole Doppler profile, provided that the quantum state of the product of interest is well selected. As the ablated products are ejected from the surface without time delay, the 2D velocity distributions of the ablated species can be obtained from measuring the single image at $v = s/t$, where s is the distance of the ablated products from

the ablation spot. The sub-Doppler resolution, nevertheless, is able to distinguish the atomic or molecular states with small energy separation (e.g., spin−orbit states of transition metals and rotational states of polyatomic molecules) because different states with distinct ν_0's will lead to different Doppler shifts that can be spatially resolved in the image due to velocity selection. This is the reason we demonstrate the sub-Doppler fluorescence images (Figure 2) in this work, although the energy separation ($\sim$15 cm^{-1})[15] between the two spin−orbit states of B($^2P^o_{3/2}$) and B($^2P^o_{1/2}$) is 30 times larger than the Doppler width ($\sim$0.5 cm^{-1}) of the ablated B atoms.

This proposed sub-Doppler fluorescence imaging method can also be applied to study laser desorption mechanisms; the experimental setup can be very similar to that depicted in Figure 1 without much modification. For laser ablation experiments, the luminous ablation plume, however, could sometimes cause problems in detecting the ablated products via LIF owing to the strong background generated with laser power above the threshold of plasma formation. Under such circumstances, factors such as the delay time between the two lasers, the position of the probe laser sheet, and the proper filters should be introduced to modify the experimental setup. On the other hand, one can use the fluorescence imaging techniques to register both the spatial distribution and the evolution of the neutral or ionic products in the laser ablation experiment performed in ambient gas pressure. For example, Cappelli et al. have reported the images of ground-state barium atoms generated by laser ablation in the presence of He background pressure.[19] It should be valuable to apply this nonintrusive method to examine the ablated products in situ during the process of pulsed laser deposition of thin films. The mechanisms of laser ablation can be revealed and the procedures of thin-film fabrication can be optimized accordingly, especially when this proposed method is used in conjunction with surface characterization of both ablated targets and deposited thin films.[11]

4. Conclusion

We have successfully applied the sub-Doppler fluorescence imaging method to study the mechanisms of the laser ablation of B atoms at 248 nm. The angular distributions of the ablated B atoms are found to be velocity-dependent, with strong forward peaking. The velocity distributions of the B atoms are bimodal, including fast and slow components. While a plasma reaction is responsible for the fast component, the slow one is caused by photochemical processes.

References and Notes

(1) Chang, J.; Chen, K.; Lin, W.; Lee, K.; Chen, Y.-T. *J. Chem. Phys.* **2000**, *113*, 5716.

(2) Zare, R. N.; Herschbach, D. R. *Proc. IEEE* **1963**, *51*, 173.

(3) Xu, Z.; Koplitz, B.; Wittig, C. *J. Chem. Phys.* **1989**, *90*, 2692.

(4) Chen, K. *Chem. Phys. Lett.* **1992**, *198*, 288.

(5) Chen K.; Pei, C. *Chem. Phys. Lett.* **1994**, *217*, 471.

(6) Chen, K.; Kuo, C.; Tzeng, M.; Shian, M.; Chung, S. E. *Chem. Phys. Lett.* **1994**, *221*, 341.

(7) Chen, K.; Sung, C.; Chang, J.; Chung, T.; Lee, K. *Chem. Phys. Lett.* **1995**, *240*, 17.

(8) Chen, K.; Lee, K.; Chang, J.; Sung, C.; Chung, T.; Liu, T.; Perng, H. *J. Phys. Chem.* **1996**, *100*, 488.

(9) Chen K.; Chang, J. *J. Phys. Chem. A* **1997**, *101*, 2525.

(10) Chen K.; Pei, C. *J. Chem. Phys.* **1998**, *109*, 6647

(11) In *Laser Ablation and Desorption*; Miller, J. C., Haglund, R. F., Jr., Eds.; Academic: San Diego, CA, 1998.

(12) In *Laser Ablation: Mechanisms and Applications*; Miller, J. C., Haglund, R. F., Jr., Eds.; Springer-Verlag: Berlin, 1991.

(13) In *Laser Ablation: Mechanisms and Applications II*; Miller, J. C., Geohegan, D. B., Eds.; AIP: New York, 1994.

(14) In *Pulsed Laser Deposition of Thin Films*; Chrisey, B., Hubler, G. K., Eds.; John Wiley & Sons: New York, 1994.

(15) Bashkin S.; Stoner, J. O. Jr. *Atomic Energy Levels and Grotrian Diagrams*; North-Holland: Amsterdam, 1975; Vol. 1.

(16) Kelly, R. *J. Chem. Phys.* **1990**, *92*, 5047.

(17) Berkowitz, J.; Chupka, W. A. *J. Chem. Phys.* **1964**, *40*, 2735.

(18) Hanley, L.; Anderson, S. L. *J. Phys. Chem.* **1987**, *91*, 5161.

(19) Cappelli, M. A.; Paul, P. H.; Hanson, R. K. *Appl. Phys. Lett.* **1990**, *56*, 1715.